X-612-69-74
PREPRINT

NASA TM X-63473

AN IMPROVED MODEL EQUATORIAL ELECTROJET WITH A MERIDIONAL CURRENT SYSTEM

M. SUGIURA
D. J. POROS

FEBRUARY 1969

GSFC

GODDARD SPACE FLIGHT CENTER
GREENBELT, MARYLAND

AN IMPROVED MODEL EQUATORIAL ELECTROJET WITH A MERIDIONAL CURRENT SYSTEM

By

M. Sugiura

Laboratory for Space Sciences
NASA-Goddard Space Flight Center
Greenbelt, Maryland 20771

and

D. J. Poros

Vitro Services
P. O. Box 385
Greenbelt, Maryland

February 1969

Presented at the Third International Symposium on Equatorial Aeronomy, Navrangpura, Ahmedabad 9, India, February 3-9, 1969

ABSTRACT

The σ_{yy} model for the equatorial electrojet presented earlier is revised by including a meridional current system, thus making the current density divergence-free. Using a spherical harmonic expansion for the geomagnetic field a model electrojet is constructed for each of the longitudes of 0°, 40°, 80°, 180°, and 280°E. It is shown that the essential feature of the meridional current system is the existence of two current loops, one on each side of the dip equator and with an equatorward current in the lower E region, an upward current over the dip equator, and a return current flowing in the upper E region. The intensities of the electrojet and the associated meridional current are significantly dependent on longitude, being strongest over Peru and weakest over India. The new model predicts a reversed (westward) current in a thin, narrow layer located at several degrees off the dip equator, which is due to a reversal of the vertical polarization field. The meridional current loop creates a toroidal magnetic field of an intensity comparable with that of the main electrojet.

INTRODUCTION

The equatorial electrojet has been a subject of extensive study both observational and theoretical. Direct observations of its magnetic field by rocket-borne magnetometers have been made by Singer et al. (1951) and Cahill (1959) in the Pacific, by Maynard et al. (1965), Maynard and Cahill (1965), and Sastry (1968) over Thumba, India, and by Davis et al. (1967) and Maynard (1967) off the coast of Peru. Numerous papers have been written on ground observations of the electrojet field; and a summary with extensive references has been given by Onwumechili (1967).

Sugiura and Cain (1966) presented a model for the equatorial electrojet which was based on the assumption that the vertical Hall current is completely inhibited everywhere by the polarization electric field. With this assumption the electrojet current density is proportional to the effective conductivity σ_{yy}, in the east-west direction, if the driving electrostatic field is uniform and eastward. This model may be regarded as the zero-th order approximation, since the current density is simply calculated using a set of given variables without solving the differential equation that a self-consistent model must satisfy. A merit of the approximation is that the realistic magnetic field configuration can readily be incorporated. Indeed, the main purpose of their paper, which will be referred to below as paper 1, was to investigate the longitudinal variation of the equatorial electrojet by using the magnetic field calculated from the spherical harmonic expansion of Jensen and Cain (1962); the height distributions of the electron density and other relevant atmospheric parameters were assumed to be independent of longitude.

However, being a zero-th order approximation the model does not exactly satisfy the differential equation to be discussed below; stated more explicitly, the current density, $\underset{\sim}{j}$, is not divergence-free, i.e., $\nabla \cdot \underset{\sim}{j} \neq 0$. Untiedt (1967) has obtained a solution that satisfies the condition $\nabla \cdot \underset{\sim}{j} = 0$; his solution includes vertical currents and consequently a meridional current system. The model, however, assumes a dipole magnetic field.

The present paper gives an improved model which satisfies $\nabla \cdot \underset{\sim}{j} = 0$ and which at the same time uses, though in a regional sense, the magnetic field configuration represented by a spherical harmonic expansion. As a new feature the model indicates that there can be a reversed, westward current in a thin layer at several degrees off, and on each side of, the dip equator. The reversed currents are essentially due to a reversal of the vertical polarization field rather than being a 'return current' from the main eastward electrojet. The magnetic field measurement made by Maynard (1967) with a magnetometer flown on a rocket off the coast of Peru has shown the existence of a reversed current similar to that predicted in the present model.

THE COORDINATE SYSTEM AND THE ASSUMPTIONS

Geocentric spherical coordinates (r, θ, ϕ) are used in this paper for the convenience of calculating the magnetic field from the spherical harmonic expansion given by Cain et al. (1967); the field is calculated for epoch 1965.0. The spherical coordinate system is defined in the following manner. Let the geographic longitude at which we wish to obtain a model for the equatorial electrojet be Λ_1. First, the geographic

colatitude, θ_1, of the dip equator at this longitude and the direction of the tangent to the dip equator at the position (θ_1, Λ_1), both on the earth's surface, are determined from the spherical harmonic expansion of the magnetic field. Then a (geocentric) spherical coordinate system is defined so that the tangent to the dip equator lies in its equatorial plane ($\theta=\pi/2$); spherical coordinates (r, θ, ϕ) used below refer to this system. Let the longitude of the point (θ_1, Λ_1) be ϕ_1 in the new spherical coordinate system. The cross section of the electrojet and the meridional current system are determined in the meridian plane of $\phi=\phi_1$. The magnitude and the direction of the magnetic field are calculated from the spherical harmonic expansion in this meridian plane as functions of r and θ. Once the magnetic field is calculated in this meridian plane we assume that the magnetic field in the model calculation is independent of ϕ. The same assumption is made with all other quantities that determine the conductivity. It is assumed that the magnetic field vector lies in the meridian plane $\phi=\phi_1$; this is a justifiable assumption near the dip equator. Since the model is intended to represent the equatorial electrojet regionally, a two-dimensional model is considered to be satisfactory. The model electrojet is assumed to be in a steady state.

THE FORMULATION

The basic equations that the electric field intensity, $\underline{E}$, and the current density, j, satisfy are

$$\nabla \times \underline{E} = 0 \qquad (1)$$

$$\nabla \cdot \underline{j} = 0 \qquad (2)$$

Equation (1) follows from the steady state condition, and (2) expresses the divergence-free current. With the condition $\partial/\partial\phi=0$, (1) gives E_ϕ and an equation for E_r and E_θ:

$$E_\phi = aE_{\phi_0}/r \sin\theta \tag{3}$$

and

$$\frac{\partial}{\partial r}(rE_\theta) - \frac{\partial E_r}{\partial \theta} = 0 \tag{4}$$

where E_{ϕ_0} is a constant, and $\underline{a}$ is the radius of the earth. Within the boundaries considered here E_ϕ is nearly constant. In Untiedt's recti-linear (plane earth) model this corresponds to the constant Ey.

The components of $\underset{\sim}{j}$ can be written as

$$j_r = (\sigma_0 \sin^2 I + \sigma_1 \cos^2 I)E_r + (\sigma_0 - \sigma_1) E_\theta \sin I \cos I - \sigma_2 E_\phi \cos I \tag{5}$$

$$j_\theta = (\sigma_0 - \sigma_1) E_r \sin I \cos I + (\sigma_0 \cos^2 I + \sigma_1 \sin^2 I) E_\theta + \sigma_2 E_\phi \sin I \tag{6}$$

$$j_\phi = \sigma_2 E_r \cos I - \sigma_2 E_\theta \sin I + \sigma_1 E_\phi \tag{7}$$

where σ_0, σ_1, and σ_2 are the direct, Pedersen, and Hall conductivities, respectively, and I is inclination of the magnetic field. Equation (7) is to be used to calculate j_ϕ when E_r and E_θ are determined from (2), (3), (4), (5), and (6).

Since $\partial/\partial\phi = 0$, it follows from (2) that in the r-θ plane j_r and j_θ can be derived from a current function ψ such that

$$j_r = -\frac{a}{r^2 \sin\theta} \frac{\partial \psi}{\partial \theta} \tag{8}$$

$$j_\theta = \frac{a}{r \sin\theta} \frac{\partial \psi}{\partial r} \tag{9}$$

From (5) and (6) together with (3), E_r and E_θ can be expressed in terms of j_r and j_θ, and hence as functions of derivatives of Ψ. Substituting these in (4) we obtain a differential equation for Ψ as follows:

$$f_1 \frac{\partial^2\Psi}{\partial r^2} + 2f_2 \frac{\partial^2\Psi}{\partial r\partial\theta} + f_3 \frac{\partial^2\Psi}{\partial\theta^2} + f_4 \frac{\partial\Psi}{\partial r} + f_5 \frac{\partial\Psi}{\partial\theta} + f_6 = 0 \qquad (10)$$

where f_1, f_2, ..., f_6 are functions of r and θ and are given by

$$f_1 = \rho_0 \cos^2 I + \rho_1 \sin^2 I$$

$$f_2 = r^{-1}(\rho_1 - \rho_0) \sin I \cos I$$

$$f_3 = r^{-2} (\rho_0 \sin^2 I + \rho_1 \cos^2 I)$$

$$f_4 = r^{-1}\left[r \frac{\partial}{\partial r} (\rho_0 \cos^2 I + \rho_1 \sin^2 I) + \frac{\partial}{\partial\theta} \{(\rho_1 - \rho_0) \sin I \cos I\}\right. \qquad (11)$$
$$\left. - (\rho_1 - \rho_0) \sin I \cos I \cot\theta\right]$$

$$f_5 = r^{-2}\left[r \frac{\partial}{\partial r} \{(\rho_1 - \rho_0) \sin I \cos I\} + \frac{\partial}{\partial\theta} (\rho_0 \sin^2 I + \rho_1 \cos^2 I)\right.$$
$$\left. - (\rho_1 - \rho_0) \sin I \cos I - (\rho_0 \sin^2 I + \rho_1 \cos^2 I) \cot\theta\right]$$

$$f_6 = - r^{-1}\left\{r \frac{\partial}{\partial r} \left(\frac{\sigma_2}{\sigma_1} \sin I\right) + \frac{\partial}{\partial\theta} \left(\frac{\sigma_2}{\sigma_1} \cos I\right) - \frac{\sigma_2}{\sigma_1} \cos I \cot\theta\right\} E_{\phi 0}$$

where $\rho_0 = 1/\sigma_0$ and $\rho_1 = 1/\sigma_1$.

THE BOUNDARY CONDITIONS

We impose the following boundary conditions: (i) $\psi=0$ at the lower ($r=r_1$) and the upper ($r=r_2$) boundaries. (ii) At the northern ($\theta=\theta_1$) and the southern ($\theta=\pi-\theta_1$) boundaries, which are far enough from the dip equator, $j_r=0$ and the θ-component of the height-integrated current is equal to the current that would be expected if the conducting layer were infinitely thin and having a conductivity equal to the height-integrated conductivity

of the layer. When the driving electric field has a ϕ-component only as in the case treated here, the latter condition reduces to that the θ-component of the height-integrated current vanishes. It is noted that the above boundary conditions become the same as those used by Untiedt (1967) in the plane-earth limit.

The condition (11) enables us to express E_θ in terms of $E_{\phi 0}$, and Ψ at $\theta=\theta_1$ and $\pi - \theta_1$ becomes

$$\Psi = E_{\phi 0} \left[\int_{r_1}^{r} \frac{\sigma_0 \sigma_2 \sin I}{\sigma_0 \sin^2 I + \sigma_1 \cos^2 I} \, dr - \frac{\int_{r_1}^{r_2} \frac{\sigma_0 \sigma_2 \sin I}{\sigma_0 \sin^2 I + \sigma_1 \cos^2 I} \frac{dr}{r}}{\int_{r_1}^{r_2} \frac{\sigma_0 \sigma_1}{\sigma_0 \sin^2 I + \sigma_1 \cos^2 I} \, dr} \int_{r_1}^{r} \frac{\sigma_0 \sigma_1}{\sigma_0 \sin^2 I + \sigma_1 \cos^2 I} \, r dr \right] \tag{12}$$

Equation (12) shows that Ψ vanishes at $r=r_1$, but that Ψ is not exactly zero at $r=r_2$. However, Ψ is nearly zero at $r=r_2$, because the two terms in (12) approximately cancel each other, and, in addition, because σ_2 and σ_1 are both nearly zero at $r=r_1$ and r_2. We could make Ψ exactly zero at $r=r_2$ by making σ_1 and σ_2 vanish at this height. In practice, however, there is little difference between the two treatments.

In the actual calculation r_1 and r_2 are chosen to represent the heights of 70 km and 380 km, respectively, and θ_1 to be 80^0, or 10^0 off the dip equator.

THE SOLUTION

The discriminant $f_2^2 - f_1 f_3$ in (10) is found to be negative, and the differential equation is of elliptic type. Equation (10) has been solved numerically by using the method of successive over-relaxation. In replacing (10) by a set of difference equations, grid points were spaced at intervals of 5 km in r and 0.5° in θ. The partial derivatives of given parameters in the coefficients f_4, f_5, f_6 were calculated numerically using a finer mesh.

The value for $E_{\phi 0}$ was taken to be 2.4×10^{-3} volts/m, which is the same as in paper 1. The solution is proportional to $E_{\phi 0}$, and hence it can be readily adjusted to different values of $E_{\phi 0}$. The electron density profile and the height distributions of σ_0, σ_1, and σ_2 are given in the Appendix. Solutions were obtained for longitudes 0°, 40°, 80°, 180°, and 280°E, roughly representing East and West Africa, India, the South Pacific, and South America, respectively. Figure 1 shows contours of equal ψ for these longitudes. Contours are drawn so that the current flowing in a (meridional) slab of thickness 1 km and between successive contours is 50 amperes. The direction of the current is upward between the two foci.

Figure 1 indicates a strong longitude dependence of the intensity of the meridional current. To make a quantitative comparison the total current (per meter-thickness) flowing between the two foci is given in Table 1 for five different longitudes; in preparing Table 1 the driving eastward electric field, $E_{\phi 0}$, is normalized to 1.0×10^{-3} volts/m, i.e., 1/2.4 times the value used for Figure 1. It can be seen from Table 1 that the meridional current is strongest over South America and weakest over India; this relation is opposite to that of the strength of the earth's magnetic field, namely, the latter is weakest over South America and strongest over India.

Table 1. The total current (in amperes per meter-thickness) flowing between the two foci and the ratio to the total current for 280°E; $E_{\phi_0} = 1.0 \times 10^{-3}$ volts/m.

Geographic longitude	Total current	Ratio
0° E	0.224	0.76
40°	0.193	0.65
80°	0.166	0.56
180°	0.228	0.77
280°	0.296	1.00

THE ELECTROJET

By numerically differentiating Ψ, j_r and j_θ can be calculated from (8) and (9); and the meridional components of the electric field can be obtained by solving (5) and (6) for E_r and E_θ. Then the eastward current j_ϕ can be determined from (7). Figure 2 shows contours of equal current intensity j_ϕ (in units of 10^{-5} amps/m^2) for longitude 280°E; the driving electric field E_{ϕ_0} is taken to be 2.4×10^{-3} volts/m. The peak current density is 5.4×10^{-5} amps/m^2, and is located at about 105 km altitude and approximately 0.3° to the south of the surface dip equator. The center of the electrojet approximately coincides with the dip equator as defined at the height of the center; at the height of 110 km the dip equator is approximately 0.3° south of that at the ground for this longitude.

An unexpected feature in the j_ϕ cross section is the existence of two thin, narrow regions at several degrees off, and on both sides of, the dip equator, in which the direction of the current is reversed. To ascertain that these are not from effects from the boundary conditions at latitudes $\pm$ 10°, the whole calculation was repeated with a new boundary condition that Ψ=0 at these boundaries. Not only did we obtain a meridional current system that is nearly identical except near the boundaries where the current is weak, we confirmed that the essential features of the j_ϕ profile is the same as in Figure 2. The region of the westward current to the south of the electrojet is larger and its intensity is stronger than the northern counterpart. This must be a result of the asymmetry of the magnetic field at this longitude. The maximum westward current intensity, located at 109 km altitude and 7° south of the dip equator,

is 0.13×10^{-5} amps/m^2, and is very much weaker than the maximum electrojet current density. Nevertheless the existence of the reversed currents is of interest, because Maynard (1967) has shown a rocket measurement of the magnetic field that suggests the presence of a reversed current at a location several degrees south of the dip equator off the coast of Peru.

The cause for the reversal in the current lies in the reversal of the vertical polarization field E_r, as is expected from (7). Figure 3 shows the height distributions of E_r for longitude 280°E. At 5° north and south of the dip equator, E_r has a very steep gradient at the altitudes of about 104 km and 114 km resulting in a hole, and a reversal, in the polarization field. The depth of the hole is found to depend on longitude; for the longitude of 80°E, the polarization field decreases roughly in the same region, but the decrease is not large enough to invert the field except in a very small area; and consequently j_ϕ is likewise not reversed, only having a steep depression, except in the small area of the inverted electric field. Figures 4 and 5 show the cross section of j_ϕ and the vertical polarization field, E_r, for longitude 80°E. Comparing Figure 4 with Figure 2 it is seen that the electrojet over India is expected to be weaker and its width to be narrower than over South America.

TOROIDAL MAGNETIC FIELDS

In a steady state, $\underset{\sim}{B}$ is related to $\underset{\sim}{j}$ by the equation

$$\nabla \times \underset{\sim}{B} = 4\pi \underset{\sim}{j}$$

From this relation together with $\partial/\partial\phi = 0$ we obtain

$$(r \sin\theta/4\pi a)\, B_\phi + \psi = \text{constant} \qquad (13)$$

Table 2. Maximum intensities of the toroidal magnetic field: for the northern and southern meridional current loops. The driving electric field: $E_\phi = 1.0 \times 10^{-3}$ volts/m.

Longitude E	Maximum intensity	
	North	South
0°	133γ	149γ
40	115	127
80	101	108
180	145	140
280	175	198

The value of ψ is zero at $r=r_1$ and r_2 and is nearly zero at the boundaries $\theta=\theta_1$ and $\pi-\theta_1$. Hence we can determine approximate intensity of the toroidal magnetic field relative to B_ϕ at the boundary. Since $r/a \simeq 1$ and $\sin\theta \simeq 1$, approximately

$$B_\phi \simeq -4\pi\psi + B_{\phi 0} \qquad (14)$$

where $B_{\phi 0}$ is B_ϕ at the boundary.

If the ψ values indicated in Figure 1 are multiplied by $4\pi \times 10^{-1} \simeq 1.25$, B_ϕ in γ is obtained. The field is westward to the north of the dip equator and is eastward to the south. The maximum values of B_ϕ, relative to the boundary value, for the longitudes of 0^o, 40^o, 80^o, 180^o, and 280^oE are given in Table 2, where the intensities are normalized to a driving electric field of 1.0×10^{-3} volts/m as in Table 1. The magnitude of the toroidal magnetic field at the center of each current loop is comparable with that of the electrojet field as observed on the ground. It will be of interest to directly observe the toroidal fields by a vector field measurement with a rocket-borne instrument. Rocket observations so far made have all been scalar measurements.

DISCUSSIONS

(1) The meridional current system presented in this paper differs from that given by Untiedt (1967) in that in our system a current loop is formed on each side of the dip equator, while in Untiedt's model the meridional current flows into the equatoral region from higher latitudes at the lower dynamo altitudes and flows out again at higher altitudes: see his Figure 2.

The difference between Untiedt's and our results is thought to stem mainly from the following circumstance. Assuming, for simplicity, a dipole

field configuration, the line of magnetic force that touches the upper boundary in our model (i.e., 380 km height) over the dip equator crosses the boundary at about 12^{o} latitude, which is very close to the northern (or southern) boundary in our calculation. While in Untiedt's model the line of force touching his upper boundary (300 km height) over the equator is cut off by the vertical boundary at about half way to its intersection with the lower boundary. Since the conductivity σ_0 along lines of force is very large, we believe that the width of 500 km in Untiedt's model is not quite adequate to obtain a reliable meridional current system. However, his model does agree with ours in gross aspects in the region within 2^{o} or 3^{o} of the dip equator.

(2) To compare the j_ϕ distribution in the new model with that in the σ_{yy} model the cross section of σ_{yy} is plotted in Figure 6 for the longitude of 280^{o}E. The half-width, as defined by the distance from the peak to one-half the peak, is about 0.7^{o} in the σ_{yy} model, while the corresponding half-width in the new model is approximately 2.5^{o}. The latter value ($\sim$ 250 km) is in rough agreement with an estimate from Figure 5 of Untiedt's paper. Over India the half-width is estimated to be about 2^{o}. In Figure 6 the peak value of σ_{yy} is 1.97×10^{-2} mho/m. With the driving electric field of 2.4×10^{-3} volts/m the maximum current density in the σ_{yy} model is 4.7×10^{-5} amps/m^2, which is slightly less than the peak current density of 5.4×10^{-5} amps/m^2 in the new model (Figure 2).

(3) Referring to Figure 3 the maximum vertical polarization field over the dip equator is at the height of 100 km and its value is approximately 25 times the driving eastward field. This large ratio of the vertical field to the eastward field is the essence of the existence of the equatorial electrojet. In the σ_{yy} model this ratio is σ_2/σ_1 over the dip equator; and the ratio is a maximum at 100 km height, its value being 28. Hence the meridional current somewhat reduces the vertical electric field but only by a small amount.

(4) In the model presented in this paper the driving electric field is assumed to be in the east-west direction. Effects of an addition of a north-south component of the electric field were investigated by including this component in the formulation, but the results indicated that this does not alter the essential features of the meridional current system. A similar conclusion has been reached by Untiedt (1967) in his model calculation.

(5) The maximum electrojet current density given here is about 5×10^{-5} amps/m^2 for the longitude of 280°E. The corresponding quantity in Untiedt's model is about 0.9×10^{-5} amps/m^2. The driving electric field used in the present model is 2.4 times the value assumed by Untiedt. The difference in the ratio σ_2/σ_1 in the two models may account for the remaining factor of about 2, though this point must be examined further in the future. When the rocket measurements were made off the coast of Peru by Maynard (1967) and Davis et al. (1967), the maximum current density over the dip equator was approximately 0.7×10^{-5} amps/m^2. Sastry (1968) measured a maximum current density of approximately 4×10^{-6} amps/m^2 over Thumba, India. Thus in both cases the observed values are smaller than

the theoretical values given here for the respective longitudes by the same factor of about 7. This difference is thought to be due mainly to weaker electric fields prevailing at the times of the rocket measurements than assumed in the model, but differences in the electron density profile and other ionospheric parameters may contribute to a certain extent.

ACKNOWLEDGEMENTS

We wish to thank Dr. N. C. Maynard for valuable discussions. We also wish to express our appreciation of Mrs. S. J. Cain's assistance in calculating the magnetic field using the spherical expansion.

APPENDIX

1. Ionospheric parameters:

The electron density profile used in the present model is shown in Figure 7. For the formulas to calculate σ_0, σ_1, and σ_2, see, for instance, Chapman (1956) or paper 1. The ionospheric parameters used in the calculation and the computed collision frequencies are listed in Table 3 for selected heights. Figure 8 shows the height distributions of σ_0, σ_1, and σ_2 over the dip equator at longitude 280°E. It is assumed that the presence of the electrojet does not affect the structure of the ionosphere.

2. Correction to paper 1:

In paper 1 (J. Geophys. Res., 71, 1869-1877, 1966) the formula for E_z in p. 1869 should read:

$$E_z = \sigma_2 \cos I/(\sigma_0 \sin^2 I + \sigma_1 \cos^2 I)$$

The error was made only in writing the equation, and no other changes are required in the rest of the paper.

Table 1. Ionospheric parameters used: neutral density, N_n; mean molecular weight, M; temperature, T; electron density, N_e; electron and ion collision frequencies, $\nu_{e,i}$.

Height	N_n	M	T	N_e	ν_e	ν_i
km	cm^{-3}		^oK	cm^{-3}	sec^{-1}	sec^{-1}
80	3.78×10^{14}	28.96	186	2.0×10^2	2.78×10^6	1.83×10^5
90	6.11×10^{13}	28.94	186	1.0×10^3	4.51×10^5	2.96×10^4
100	1.04×10^{13}	28.30	208	1.0×10^5	8.24×10^4	5.08×10^3
110	2.11×10^{12}	27.73	245	1.7×10^5	1.99×10^4	1.05×10^3
120	5.47×10^{11}	26.97	295	2.0×10^5	6.76×10^3	2.74×10^2
130	1.51×10^{11}	26.25	466	2.1×10^5	2.70×10^3	7.66×10
140	6.09×10^{10}	25.71	693	2.0×10^5	1.39×10^3	3.12×10
150	3.33×10^{10}	25.28	880	2.1×10^5	9.16×10^2	1.72×10
160	2.18×10^{10}	24.89	997	2.2×10^5	7.16×10^2	1.14×10
180	1.14×10^{10}	24.17	1140	2.7×10^5	5.56×10^2	6.03
200	6.85×10^9	23.47	1213	3.3×10^5	5.16×10^2	3.68
220	4.39×10^9	22.78	1251	3.8×10^5	5.09×10^2	2.39
240	2.91×10^9	22.11	1275	4.5×10^5	5.44×10^2	1.61
260	1.99×10^9	21.44	1286	5.0×10^5	5.72×10^2	1.12
280	1.39×10^9	20.81	1294	4.8×10^5	5.35×10^2	7.93×10^{-1}
300	9.83×10^8	20.21	1299	4.5×10^5	4.94×10^2	5.69×10^{-1}
350	4.41×10^8	18.91	1300	3.2×10^5	3.50×10^2	2.64×10^{-1}

REFERENCES

Cahill, L. J., Jr., Investigation of the equatorial electrojet by rocket magnetometer, J. Geophys. Res., 64, 489-501, 1959.

Cain, J. C., S. J. Hendricks, R. A. Langel, and W. V. Hudson, A proposed model for the International Geomagnetic Reference Field-1965*, J. Geomag. Geoelec., 19, 335-355, 1967.

Chapman, S., The electrical conductivity of the ionosphere: a review, Nuo o Cimento, Suppl. 4 [10], 4, 1385-1412, 1956.

Davis, T. N., K. Burrows, and J. D. Stolarik, A latitude survey of the equatorial electrojet with rocket-borne magnetometers, J. Geophys. Res., 72, 1845-1861, 1967.

Jensen, D. C., and J. C. Cain, An interim geomagnetic field (abstract), J. Geophys. Res., 67, 3568-3569, 1962.

Maynard, N. C., Measurements of ionospheric currents off the coast of Peru, J. Geophys. Res., 72, 1861-1875, 1967.

Maynard, N. C., and L. J. Cahill, Jr., Measurement of the equatorial electrojet over India, J. Geophys. Res., 70, 5923-5936, 1965.

Maynard, N. C., L. J. Cahill, Jr., and T. S. G. Sastry, Preliminary results of measurements of the equatorial electrojet over India, J. Geophys. Res., 70, 1241-1245, 1965.

Onwumechilli, A., Geomagnetic variations in the equatorial zone, in Physics of Geomagnetic Phenomena, S. Matsushita and W. H. Campbell, eds., Academic Press, New York, 425-507, 1967.

Sastry, T. S. G., Quiet-day electrojet over Thumba, India, J. Geophys. Res., 73, 1789-1794, 1968.

Singer, S. F., E. Maple, and W. A. Bowen, Evidence for ionospheric currents from rocket experiments near the geomagnetic equator, J. Geophys. Res., 56, 265-281, 1951.

Sugiura, M , and J. C. Cain, A model equatorial electrojet, J. Geophys. Res., 71, 1869-1877, 1966.

Untiedt, J., A model of the equatorial electrojet involving meridional currents, J. Geophys. Res., 72, 5799-5810, 1967.

FIGURE CAPTIONS

Figure 1. The flow pattern of the meridional current associated with the equatorial electrojet for different longitudes. The current flowing between successive contours is 50 amperes per km thickness. The driving electric field, $E_{\phi o}$=2.4 x 10^{-3} volts/m. The current flows upward over the dip equator.

Figure 2 The eastward current density, j_ϕ, for longitude 280°E; in units of 10^{-5} amp/m^2. The driving electric field, $E_{\phi o}$= 2.4 x 10^{-3} volts/m. The shaded areas represent reversed, westward currents.

Figure 3. The vertical polarization field, E_r, directly over the dip equator and at 5° north and south of the dip equator: for 280°E longitude. The driving electric field, $E_{\phi o}$= 2.4 x 10^{-3} volts/m.

Figure 4. The eastward current density, j_ϕ, for longitude 80°E: in units of 10^{-5} amp/m^2. The driving electric field, $E_{\phi o}$ = 2.4 x 10^{-3} volts/m. The shaded areas represent reversed, westward currents.

Figure 5. The vertical polarization field, E_r, directly over the dip equator and at 5° north and south of the dip equator: for 80°E longitude; $E_{\phi o}$ = 2.4 x 10^{-3} volts/m.

Figure 6. The σ_{yy} profile: in units of 10^{-4} mho/m. The peak value is 1.97 x 10^{-2} mho/m.

Figure 7. The electron density profile used in the model.

Figure 8. Conductivities σ_o, σ_1, and σ_2 as functions of height, over the dip equator and for the longitude of 280°E.

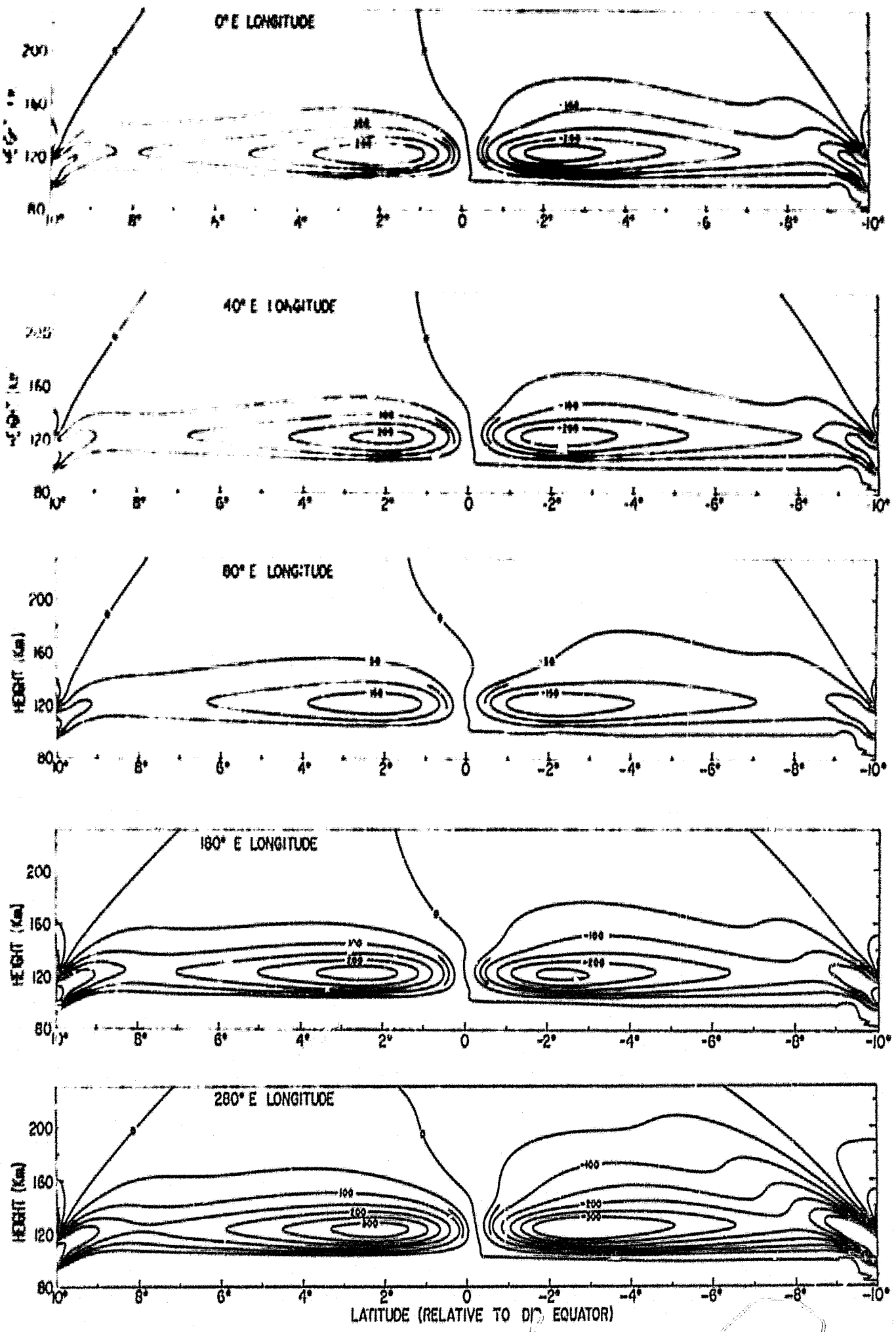
0° E LONGITUDE
40° E LONGITUDE
80° E LONGITUDE
180° E LONGITUDE
280° E LONGITUDE
HEIGHT (Km)
200
160
120
80
10°
8°
6°
4°
2°
0
-2°
-4°
-6°
-8°
-10°
LATITUDE (RELATIVE TO DIP EQUATOR)

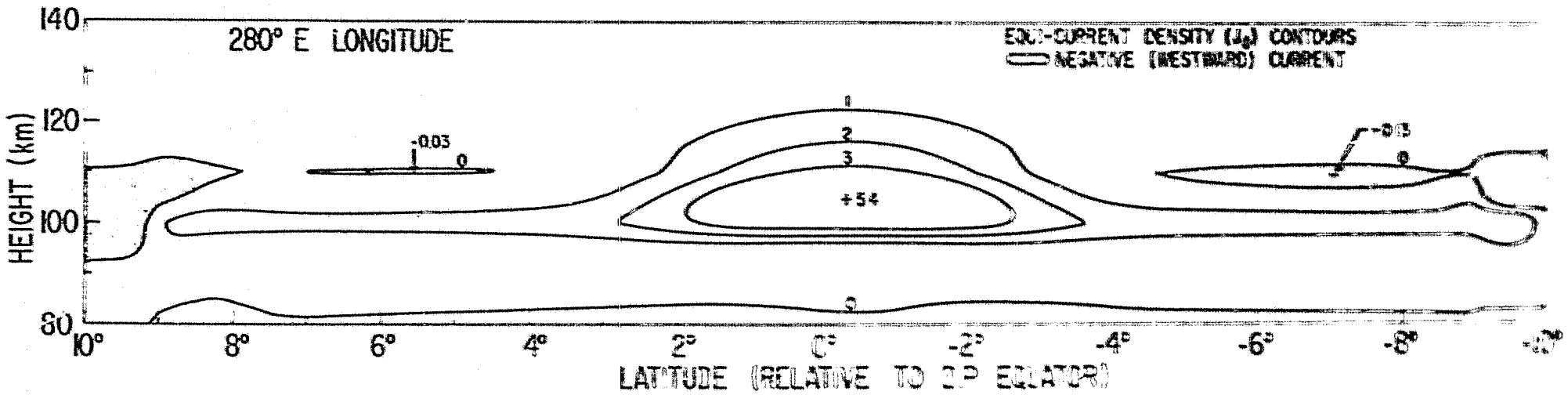
140
120
100
80
HEIGHT (km)
280° E LONGITUDE
EQU-CURRENT DENSITY (J_ϕ) CONTOURS
NEGATIVE (WESTWARD) CURRENT
-0.03
0
1
2
3
+54
10°
8°
6°
4°
2°
0°
-2°
-4°
-6°
-8°
LATITUDE (RELATIVE TO 2° EQUATOR)

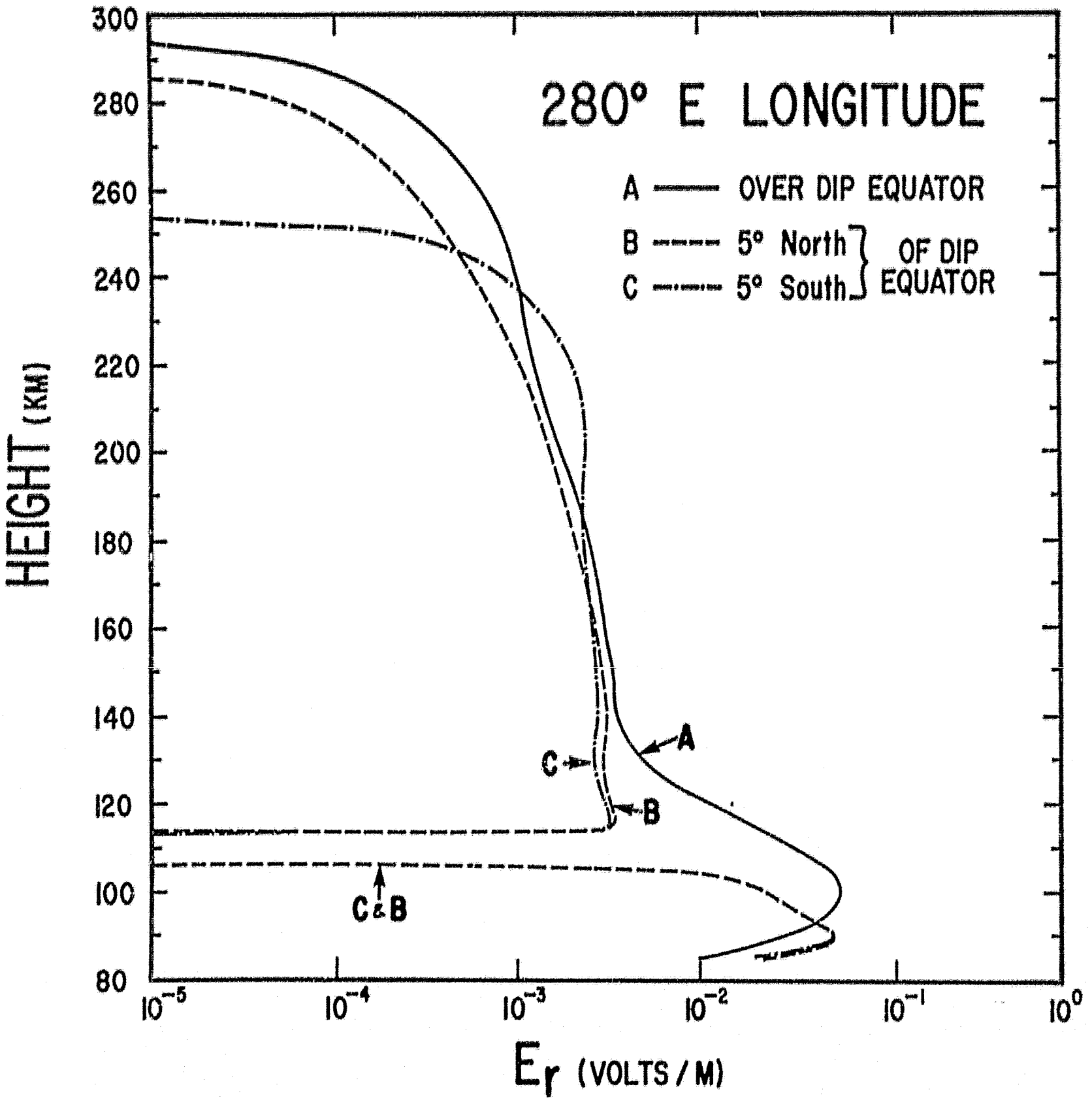
280° E LONGITUDE
A —— OVER DIP EQUATOR
B ---- 5° North } OF DIP
C -·-·- 5° South } EQUATOR
HEIGHT (KM)
300
280
260
240
220
200
180
160
140
120
100
80
A
C
B
C & B
10^{-5}
10^{-4}
10^{-3}
10^{-2}
10^{-1}
10^{0}
E_r (VOLTS / M)

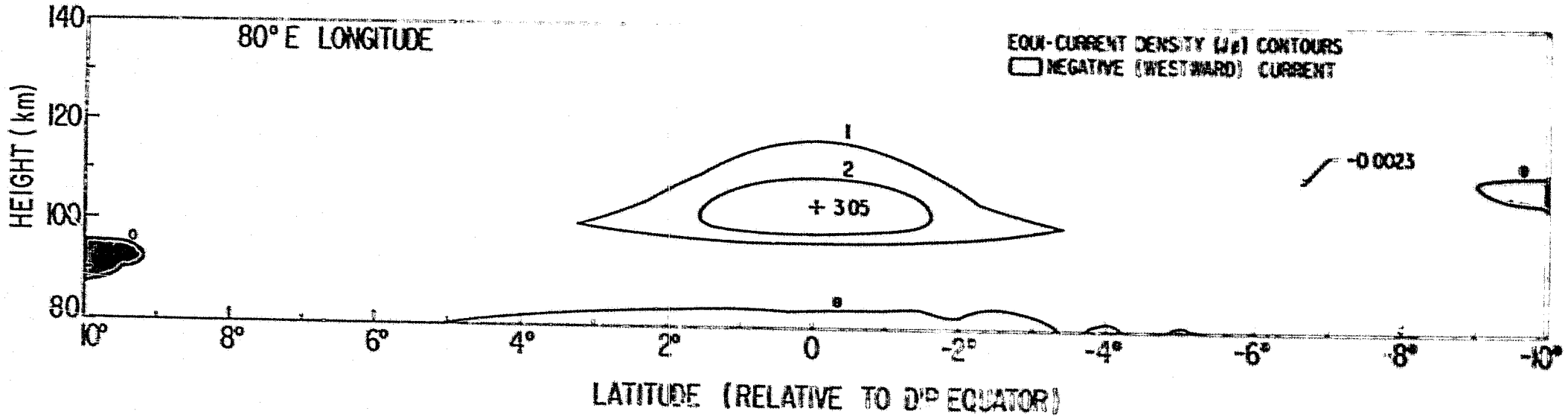
80° E LONGITUDE
EQUI-CURRENT DENSITY (μA) CONTOURS
NEGATIVE (WESTWARD) CURRENT
HEIGHT (km)
140
120
100
80
1
2
+ 305
-0 0023
10°
8°
6°
4°
2°
0
-2°
-4°
-6°
-8°
-10°
LATITUDE (RELATIVE TO DIP EQUATOR)

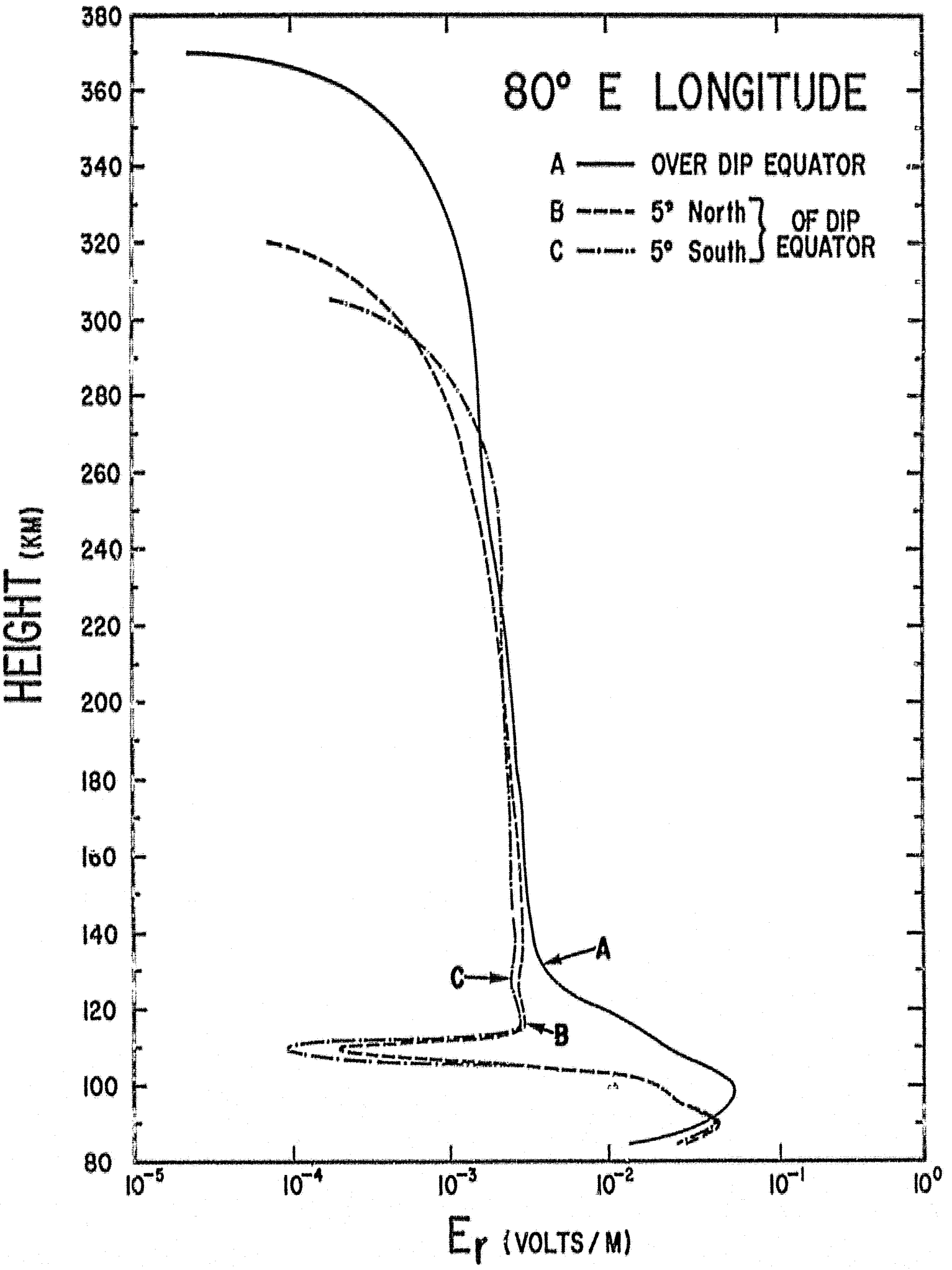
80° E LONGITUDE
A —— OVER DIP EQUATOR
B ---- 5° North } OF DIP
C -·-·- 5° South } EQUATOR
HEIGHT (KM)
380
360
340
320
300
280
260
240
220
200
180
160
140
120
100
80
10⁻⁵
10⁻⁴
10⁻³
10⁻²
10⁻¹
10⁰
Er (VOLTS/M)
A
B
C

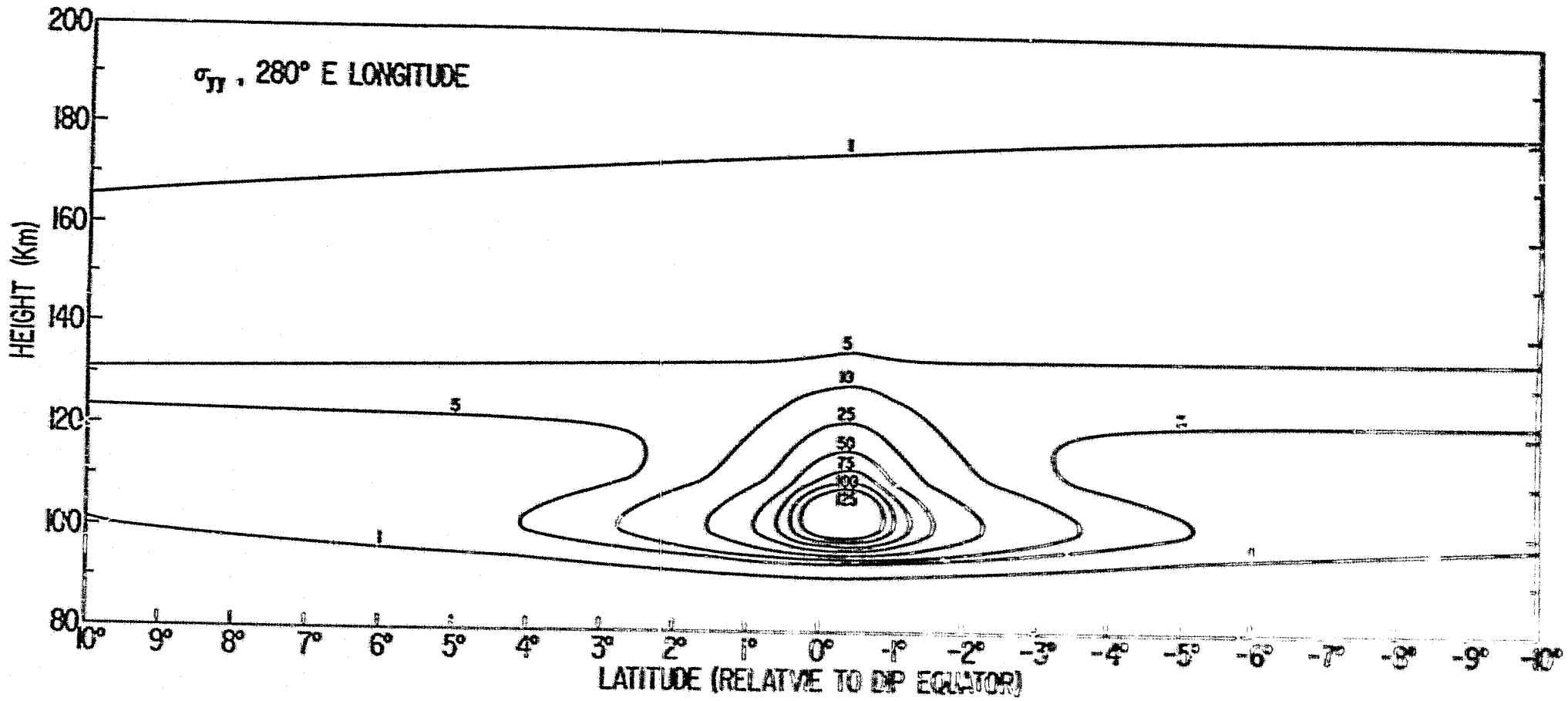
σ_{yy} , 280° E LONGITUDE
HEIGHT (Km)
200
180
160
140
120
100
80
1
5
10
25
50
75
100
125
10° 9° 8° 7° 6° 5° 4° 3° 2° 1° 0° -1° -2° -3° -4° -5° -6° -7° -8° -9° -10°
LATITUDE (RELATIVE TO DIP EQUATOR)

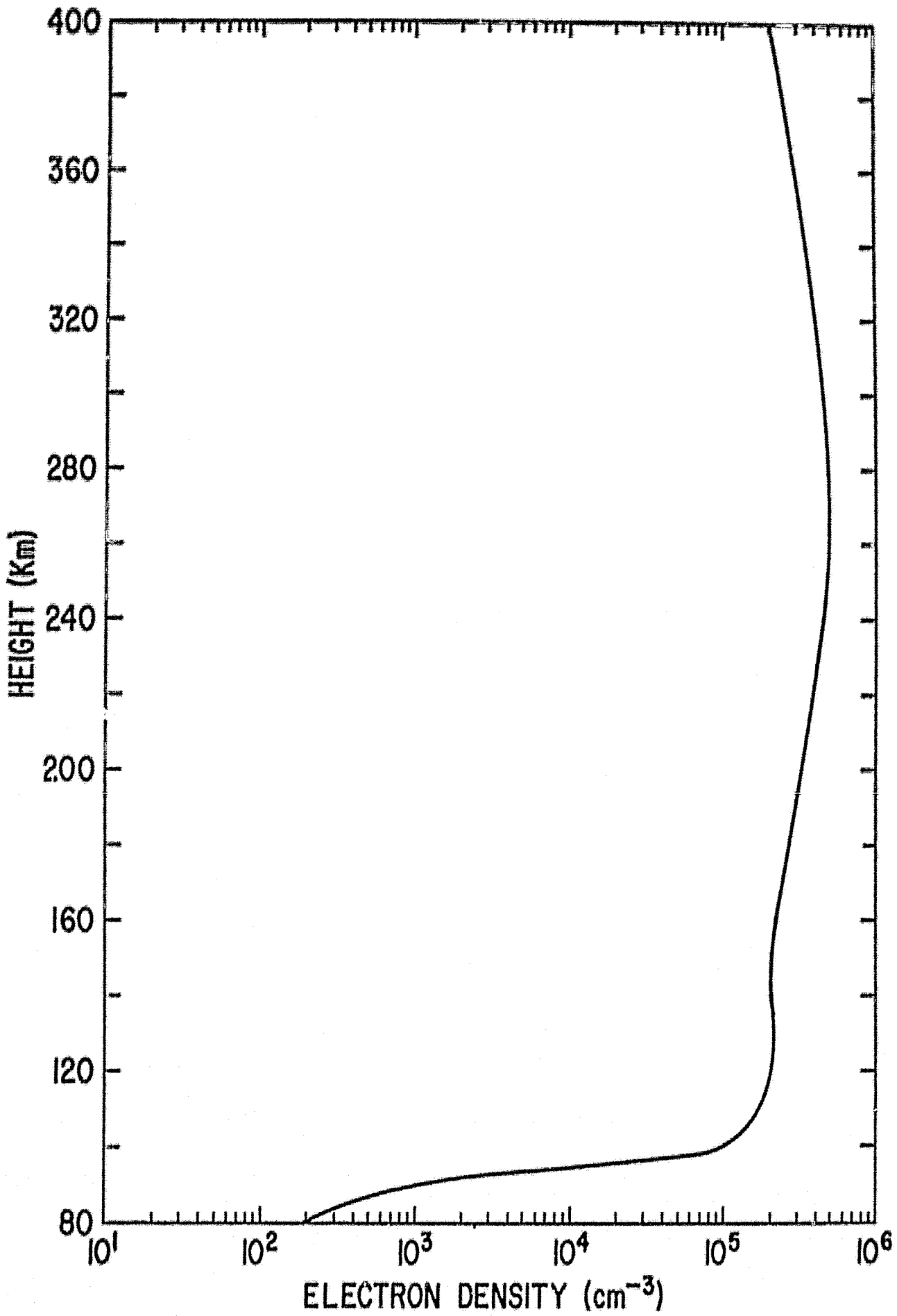
400
360
320
280
240
200
160
120
80
HEIGHT (Km)
10^1
10^2
10^3
10^4
10^5
10^6
ELECTRON DENSITY (cm^{-3})

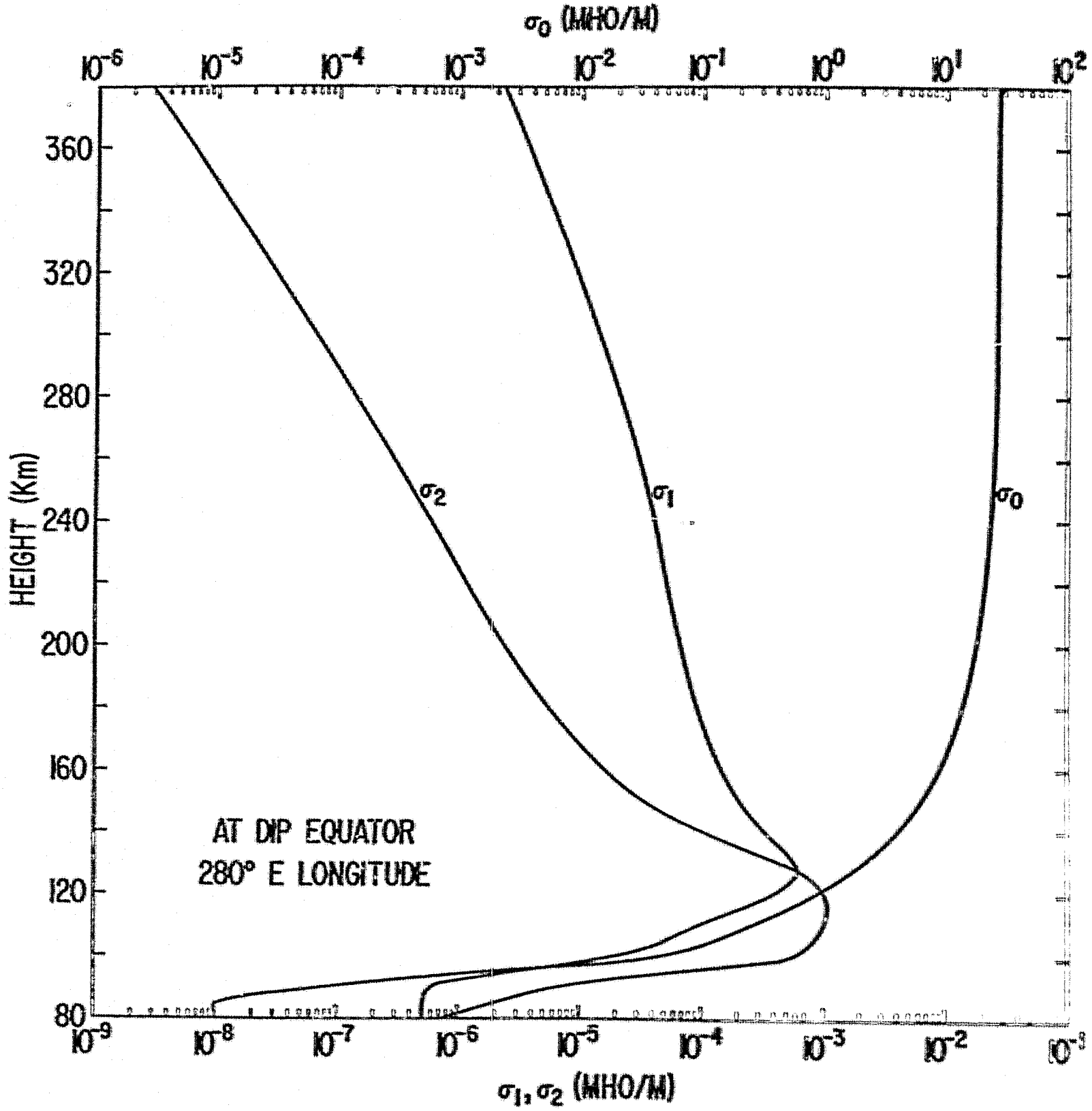
σ_0 (MHO/M)
10^{-6}
10^{-5}
10^{-4}
10^{-3}
10^{-2}
10^{-1}
10^{0}
10^{1}
10^{2}
360
320
280
240
200
160
120
80
HEIGHT (Km)
σ_2
σ_1
σ_0
AT DIP EQUATOR
280° E LONGITUDE
10^{-9}
10^{-8}
10^{-7}
10^{-6}
10^{-5}
10^{-4}
10^{-3}
10^{-2}
σ_1, σ_2 (MHO/M)